IOP Publishing Journal of Physics: Condensed Matter

J. Phys.: Condens. Matter **20** (2008) 494219 (9pp) doi:10.1088/0953-8984/20/49/494219

Kinetics of sedimentation in colloidal suspensions

Stefano Buzzaccaro, Antonio Tripodi, Roberto Rusconi[1], Daniele Vigolo and Roberto Piazza

Dipartimento di Chimica, Materiali e Ingegneria Chimica, Politecnico di Milano, Italy

E-mail: roberto.piazza@polimi.it

Received 1 August 2008
Published 12 November 2008
Online at stacks.iop.org/JPhysCM/20/494219

Abstract

Measuring the concentration profiles induced by gravity settling is known to be an efficient route to obtain the equation of state of a colloidal suspension, to inspect the fine details of the phase diagram and to provide clues on the nature of metastable phases. Here we show that a careful analysis of the transient settling profiles may add valuable information for what concerns colloidal hydrodynamics. In particular, we show that a numerical inversion of a kinetic profile yields the full hydrodynamic factor $K(\Phi)$ up to the concentration of the original unsettled suspension, and that the dilute part of the profile yields a 'dynamic' gravitation length also related to $K(\Phi)$. These predictions are tested on a suspension of monodisperse hard and sticky spheres. Finally we describe and test a novel optical method, allowing us to measure sedimentation profiles on a wide class of colloidal systems, even in the presence of a noticeable turbidity.

1. Introduction

Sedimentation processes are ubiquitous in nature and important for technology and science. Clarifiers and gravity settlers are commonly used to separate particles from wastestreams and, in lab practice, analytical ultracentrifugation is a common tool to separate or characterize particle size distribution [1]. Yet, besides their practical interest, sedimentation studies on model systems have also provided fundamental information on the structural properties of colloidal suspensions. More than 80 years after the celebrated work by Perrin [2], which gave crucial experimental support to the Einstein theory of Brownian motion, measurements of equilibrium sedimentation profiles by depolarized light scattering [3] or X-ray adsorption [4] have allowed us to obtain the full equation of state for hard spheres (HS). Following these seminal investigations, we have recently shown that sedimentation studies can accurately yield the equation of state and phase diagram of a suspension of particles which, due to the presence of a depletion agent, behave as adhesive hard spheres (AHS), and can also provide crucial information on the occurrence and structural properties of metastable gel phases that form in the presence of sufficiently strong depletion interactions [5]. In particular, we provided clear evidence that gelation in a depletion system is always associated with an arrested liquid–liquid phase separation, a conclusion recently and amply supported by confocal microscopy and numerical simulation [6].

Exploiting sedimentation to extract facts and figures on the equilibrium phase behaviour may then be regarded as a consolidated experimental approach. Conversely, aside from standard measurements of the sedimentation velocity made by tracking the meniscus separating a settling suspension from the supernatant, little attention has so far been paid to quantitative studies of the sedimentation kinetics[2]. In this work, we plan to show that transient settling profiles can give crucial information on the hydrodynamics of colloidal suspensions. Specifically, we show that a simple numerical inversion of the time-invariant shape that a sedimentation profile assumes after a sufficiently long transient directly yields the dependence of the sedimentation velocity v on the particle volume fraction Φ, provided that the equation of state $\Pi(\Phi)$, where Π is the suspension osmotic pressure, is known. Conversely, when the former is already known from settling speed measurements, $\Pi(\Phi)$ can be extracted without the need for long equilibration

[1] Present address: SEAS, Harvard University, USA.

[2] A noticeable exception is the analysis of the long-wavelength, unscreened velocity fluctuations taking place in the sedimentation of non-Brownian particles [7, 8].

times. In particular, we stress the concept of a 'dynamic sedimentation length', describing the dilute top region of a settling profile and directly related to $v(\Phi_0)$, where Φ_0 is the volume fraction of the homogeneous unsettled suspension. Finally, we describe a novel experimental method, based on tracking along the profile the deflection of a laser beam which, besides granting an easier inversion of the settling profile, allows extending quantitative measurements of sedimentation profiles to a wide class of colloidal systems. These concepts and methods are tested on a suspension of monodisperse hard and sticky spheres.

2. Sedimentation kinetics

Let us first recall some basic aspects of gravity settling for interacting colloids. Consider a dispersion of spherical particles with radius R and material density ρ_p, sedimenting along the z axis (taken antiparallel to $\mathbf{g}$) in a solvent of density ρ_s and viscosity η. The particle settling velocity is found by balancing the viscous drag with the total force F_z acting on a particle, which is given by the sum of the buoyancy and osmotic contributions:

$$F_z = -gV_p\Delta\rho - \frac{V_p}{\Phi}\frac{\partial\Pi}{\partial z}, \tag{1}$$

where $\Delta\rho = \rho_p - \rho_s$, V_p is the particle volume, $\Phi = \Phi(z,t)$ is the space/time-dependent particle volume fraction profile and Π is taken as a functional of $\Phi(z,t)$.

It is convenient writing v_z as $v_z = \mu_0 K(\Phi) F_z$, where the factor $K(\Phi)$ accounts for hydrodynamic interaction effects on the particle mobility μ, whose single-particle limit is $\mu_0 = (6\pi\eta R)^{-1}$. The mass flux J_z along z is then given by

$$J_z = \Phi v = \Phi\mu_0 V_p K(\Phi)\left[-g\Delta\rho - \frac{1}{\Phi}\frac{\partial\Pi}{\partial z}\right]. \tag{2}$$

By writing the osmotic pressure as $\Pi(\Phi) = (k_BT/V_p)\Phi Z(\Phi)$, where the compressibility factor $Z(\Phi)$ accounts for interparticle interactions, and $D_0 = \mu_0 k_BT$, $v_S = \mu_0 g\Delta\rho V_p$ for the dilute limits of, respectively, the diffusion coefficient and sedimentation velocity, we then have

$$J_z = -\Phi v_S K(\Phi) - D_0 K(\Phi)\frac{\partial[\Phi Z(\Phi)]}{\partial\Phi}\frac{\partial\Phi}{\partial z}. \tag{3}$$

The continuity equation $\partial_t\Phi(z,t) = -\partial_z J_z(z,t)$ finally yields

$$\frac{\partial\Phi}{\partial t} - v_S\frac{\partial[\Phi K(\Phi)]}{\partial z} = D_0\frac{\partial}{\partial z}\left\{K(\Phi)\frac{\partial[\Phi Z(\Phi)]}{\partial\Phi}\frac{\partial\Phi}{\partial z}\right\}. \tag{4}$$

If at $t = 0$ the suspension has a uniform volume fraction Φ_0 and fills the cell up to a height h, the time-dependent concentration profile is found from equation (4) with the boundary condition that the flux vanishes at $z = 0, h$.

2.1. Equilibrium

At equilibrium the mass flux vanishes so that, from equation (2)

$$\frac{\partial\Pi}{\partial z} = -\Delta\rho g\Phi. \tag{5}$$

A simple integration yields

$$\Pi(z) = \Delta\rho g\int_z^\infty \Phi(z')\,dz'. \tag{6}$$

Equation (6) simply states that, at equilibrium, the osmotic pressure at a given height z balances the total weight per unit area of the particles lying above that point. By a z scan of the concentration profile it is therefore possible to obtain $\Pi(\Phi)$, i.e. the whole equation of state of the system. In the dilute limit, with $Z(\Phi) \equiv 1$, equation (5) yields the barometric law for ideal gases $\Phi(z) = C\exp(-z/\ell_g)$, where the gravitational length ℓ_g is given by

$$\ell_g = \frac{k_BT}{g\Delta\rho V_p}. \tag{7}$$

For what follows, it is also useful noticing that ℓ_g is also equal to the ratio D_0/v_S between the single-particle diffusion coefficient and the Stokes sedimentation velocity, and may be seen as the distance a particle has to settle before the sedimentation drift becomes equal to the rms displacement due to Brownian motion. In the next section, we show that, after sufficiently long time, non-equilibrium profiles are also characterized by a 'dynamic' gravitational length ℓ_g^{dyn}, which is proportional to ℓ_g, but also embodies important information on hydrodynamic interactions.

2.2. Settling profile

Three distinct regions can be qualitatively distinguished in the settling profile of a suspension, initially at uniform volume fraction Φ_0 [9]:

- a supernatant region, essentially devoid of particles, at the top of the cell (region I);
- a uniform column where $\Phi = \Phi_0$, connected to region I by a more or less expanded 'fan' (region II);
- a dense (possibly crystalline) sediment close to the cell bottom (region III).

Here we shall focus only on the fan region. Equation (4) has a Burgers-like structure. This means that, for any smooth initial condition $\Phi(-\infty,t) = \Phi_0$ and $\Phi(\infty,t) = 0$, the late-time asymptotic profile is a shock front moving with constant speed and shape [10]. Indeed, substituting $\Phi(z,t) = \Phi(z+vt)$ into (4) and integrating from z to infinity, we have

$$D_0 K(\Phi)\frac{\partial[\Phi Z(\Phi)]}{\partial\Phi}\frac{\partial\Phi}{\partial z} = [v - K(\Phi)v_S]\Phi, \tag{8}$$

which for large negative z gives $v = v(\Phi_0) = K(\Phi_0)v_S$. This steady-state, time-invariant profile, which may not be so intuitive, is in fact a direct consequence of the dependence of settling velocity on particle concentration. Were it not for this effect, an initially sharp profile, settling with a constant velocity $v(\Phi_0)$, would spread out due to diffusion. Conversely, since $v(\Phi)$ is a monotonically decreasing function of Φ, those particles which are 'left behind' by diffusion sediment faster, catching up with the front region of the settling profile, which therefore self-sharpens. Yet, this tendency for the particles at

the top of the fan (sedimenting with $v \simeq v_S$) to merge with the lower-lying suspension (settling at the constant velocity $v(\Phi_0) < v_S$) is counteracted by an osmotic pressure gradient, which does not fully balance buoyancy as in equilibrium, but still slows them down. Eventually, this leads to a time-invariant shape, dictated by the balance between settling and diffusion and settling at the uniform speed $v(\Phi_0)$. The physics of the problem can be better grasped by considering a reference frame co-moving with the uniform settling column. In this frame, the top of the column expands due both to diffusion *and* to the drag force exerted by the fluid, which is uniformly moving upwards with speed $v(\Phi_0)$. The steady-state profile, therefore, does not coincide with the equilibrium one, but rather with what would be obtained in a fluidized bed, where a laminar solvent flow from the bottom is imposed [11].

At this point, we have however assumed to deal with a semi-infinite settling column (not bounded below by the cell bottom). In real conditions, whether or not the time-invariant state is actually reached depends on the cell height, because region II may merge with region III (the thick sediment) long before this steady-state condition is reached. To settle this point, a quantitative analysis of the specific experimental conditions is mandatory. In fact, as we shall see, for a very dilute system, the stationary state is actually a uniform profile spanning the whole cell, which obviously cannot be reached before the constant-Φ column merges with the sediment. This means that, for a given cell height, there exists a minimal initial concentration below which the profile cannot reach a time-invariant shape.

The exact shape of the stationary profile depends on the specific interparticle interactions, and can be obtained only numerically. Since collective effects on $v(\Phi)$ and $D(\Phi)$ differ (in particular the latter, besides depending on hydrodynamic interactions such as $v(\Phi)$, is also inversely proportional to the osmotic compressibility), the specific shape of the time-invariant profile bears relevant information on direct and hydrodynamic interparticle interactions. Particularly interesting from an experimental point of view is that equation (8) allows us to extract extensive *dynamic* information, such as the whole behaviour of $K(\Phi)$ up to Φ_0, from a *single static* measurement. Indeed, rearranging equation (8) as

$$\frac{K(\Phi)}{K(\Phi_0)} = \left[1 + \ell_g \frac{\partial(\Phi Z(\Phi))}{\partial \Phi} \frac{\partial \Phi}{\partial z} \Phi^{-1}\right]^{-1}, \qquad (9)$$

we see that all quantities on the right-hand side are directly measurable, either from the settling profile ($\Phi(z)$ and its derivative) or from equilibrium measurements ($Z(\Phi)$). Taking into account that, since $\lim_{\Phi\to 0} K(\Phi) \equiv 1$, the dilute limit of the right-hand side is simply equal to $K(\Phi_0)^{-1}$, equation (9) allows us therefore to evaluate the full concentration dependence of the hydrodynamic factor up to Φ_0. To appreciate the effectiveness of this approach, it is useful to observe that 'standard' measurements of $K(\Phi)$ by dynamic light scattering require us first of all to extrapolate to zero wavevector q the diffusion coefficient $D(q, \Phi)$ for many samples at different concentrations, and then to evaluate $K(\Phi) = D(0, \Phi)S(0, \Phi)$ using the $q = 0$ limit of the structure factor $S(q, \Phi)$ that can be obtained by static scattering measurements at small scattering angle. To make things worse, for systems of colloidal particles interacting with repulsive forces such as HS, the concentration dependence of $D(\Phi)$ is generally weaker than for $K(\Phi)$, since the osmotic compressibility decreases with Φ.[3] Unfortunately, as we shall see, obtaining $K(\Phi)$ from depolarized scattering measurements, such as those used in [3, 5], requires us to differentiate the experimental profile, a procedure that unavoidably introduces sensible numerical noise. In section 3.3 we shall introduce a different optical method, yielding much better results.

We shall now briefly dwell upon some general consideration of the functional form of a time-invariant settling profile in the region at the top of the fan where $\Phi \ll \Phi_0$ which, to our knowledge, has so far passed unnoticed, but may yield ready-to-use information of the suspension dynamics. For $\Phi \to 0$, we can approximate $K(\Phi) \simeq 1$ and $Z(\Phi) \simeq 1$, so that equation (8) becomes

$$\frac{\partial \Phi}{\partial z} = \frac{v_S[K(\Phi_0) - 1]}{D_0}\Phi = -\frac{\Phi}{\ell_g^{dyn}(\Phi_0)}, \qquad (10)$$

where we have defined a *dynamic* gravitational length:

$$\ell_g^{dyn}(\Phi_0) = \frac{\ell_g}{1 - K(\Phi_0)} \qquad (11)$$

which depends only on the initial particle volume fraction. Therefore, as for the equilibrium profile, the top part of the profile still has an exponential (barometric) shape, but fixed by the *new* length scale ℓ_g^{dyn} which is always *larger* than ℓ_g because $K(\Phi) < 1$. This result is particularly interesting, since it shows that direct information on colloidal hydrodynamic interactions can be obtained with a simple *static* measurement of a settling profile (or, analogously, by fluidizing an already equilibrated sedimentation profile). As we shall see, it may have some relevance in explaining the alleged 'anomalies' in ℓ_g reported in [3]. Since $K(\Phi)$ is generally a monotonic decreasing function of Φ, ℓ_g^{dyn} gets larger for smaller Φ_0. The stationary profile for a dilute solution is then very expanded and, in the limit of $\Phi_0 \to 0$ $\ell_g^{dyn} \to \infty$ (uniform profile). In passing, we notice that a limiting exponential shape of the profile, characterized by a second dynamic gravitational length $(\ell_g^{dyn})'$, is also found for $\Phi \to \Phi_0$. Since the expression for $(\ell_g^{dyn})'$ is much more involved, this result is, however, of lesser experimental avail.

To make the former results explicit, we present some numerical data obtained by solving equation (8) using a finite-element routine with an auto-adaptive mesh (*FlexPde 5*, PDE Solutions Inc.). Figure 1 shows the time evolution of a settling profile for HS of radius $R = 77$ nm, with an initial condition corresponding to a homogeneous suspension at $\Phi_0 = 0.23$, filling the cell up to a height $h = 3.6$ cm. Since we are interested only in a moderately concentrated fluid region, to speed up the calculation we assumed the Carnahan–Starling

[3] Of course, light scattering measurements give access to much richer information, yielding the full dynamic structure factor and not just its hydrodynamic limit.

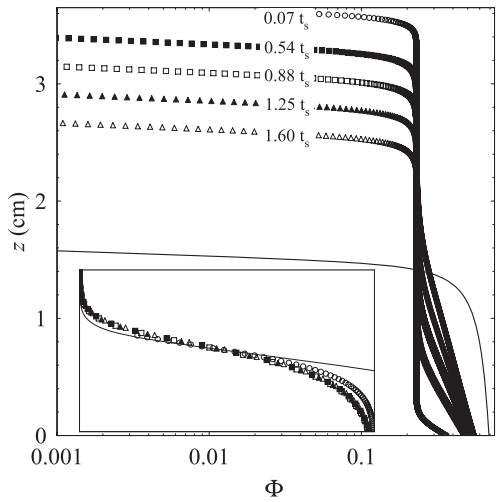

Figure 1. Numerical results for the sedimentation profiles of an HS suspension at initial volume fraction $\Phi_0 = 0.23$. Settling time is expressed in units of the Stokes time $t_S = h/v_S$. The full line is the equilibrium profile, obtained for $t > 20t_S$. The fans of the profiles are superimposed in the inset.

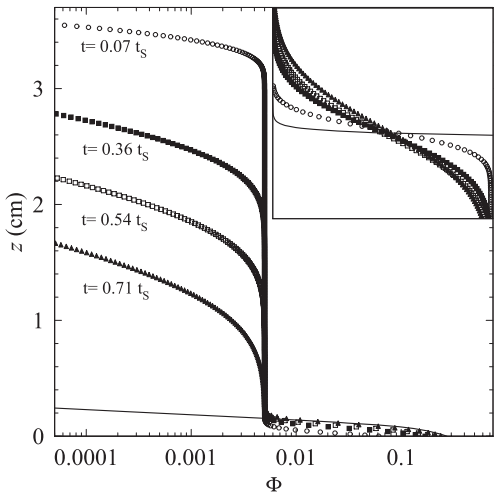

Figure 2. Numerical sedimentation profiles for an HS suspension at initial volume fraction $\Phi_0 = 5 \times 10^{-3}$. The full line is the equilibrium profile. The inset shows that, for this low initial volume fraction, the fans do not superimpose, but rather get more and more expanded as the settling time goes by.

(CS) equation of state for HS [12] to be valid up to the close-packing limit (therefore, the profile region where $\Phi > 0.49$ is not physically meaningful, and the simulation may be assumed to hold only before regions II and III significantly merge). For what concerns the hydrodynamic factor, we used the semi-empirical expression $K(\Phi) = (1 - \Phi)^{6.55}$ [9].

The log plot in the main body of figure 1 shows that the top part of the profiles has an exponential trend, characterized by a dynamic gravitation length $\ell_g^{dyn} > \ell_g$. The top parts of the profiles (the 'fans'), which are superimposed in the inset, show that the latter reach a time-invariant shape after a time $t \geqslant 0.2$–$0.3\ t_S$. Conversely, the numerical results obtained for a very dilute suspension ($\Phi_o = 5 \times 10^{-3}$), shown in figure 2, show that no steady-state profile is reached before the constant-Φ column and the sediment merge. Rather, the fan gets more and more expanded with time, until regions II and III merge and the profile gradually subsides over the equilibrium one. In figure 3 we plot the apparent sedimentation length l_g^* that one would extract from the slope of the upper exponential part of the profiles as a function of the settling time. The figure shows that ℓ_g approaches ℓ_g^{dyn} exponentially, with a rate $1/k$ that grows with the initial volume fraction Φ_0. A rapid decrease of ℓ_g^* to the equilibrium value ℓ_g takes place only after regions II and III start to merge, although differences can still be appreciated for t as long as $5t_S$.

Before describing our experimental results, it is timely making a short digression to show how the former considerations may partially account for the alleged 'anomalous' sedimentation effects reported in [3]. In that work, the authors describe two kinds of experiments. The first one refers to a suspension of fluorinated particles (see section 3) whose sedimentation profiles was followed for about $4.5t_S$ before obtaining, from what was considered an equilibrium profile, the first experimental measurement of the equation of state for hard spheres. The results showed, however, two puzzling

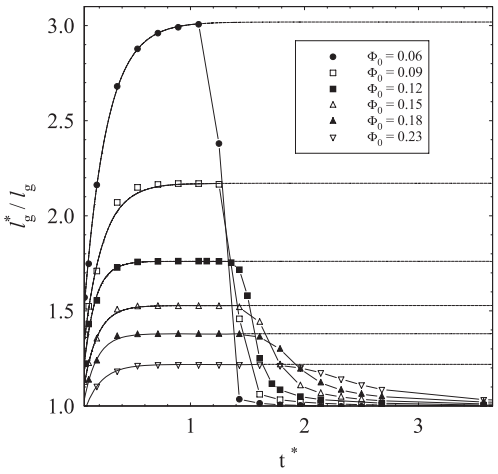

Figure 3. Apparent gravitational length ℓ_g^* as a function of the normalized settling time $t^* = t/t_S$ for different initial volume fractions. The initial rising regions are fitted as $\ell_g^* = \ell_g^{dyn}[1 - c\exp(-kt^*)]$. The dashed lines indicate the asymptotic dynamic sedimentation length, given by equation (11). When regions II and III start to merge ($t^* \simeq 1$–1.5), ℓ_g^* shows a rapid decrease to the equilibrium value ℓ_g.

aspects. First of all, the fluid branch of the profile did comply with the CS equation of state, but with a gravitational length that was about 30% larger than the calculated value. Moreover, the osmotic pressure of the colloidal crystal branch did not fit at all the theoretical predictions. Neither of these anomalies was found in our recent experiments [5], which conversely yield an extremely good quantitative agreement for both the fluid and crystal phases. To enquire about this fact, we re-examined the full time dependence of the settling profiles obtained back in 1993 for this sample, which are luckily still available in the fatigued, but still working, hard disk of a Macintosh SE30. In the data, the apparent gravitation length shows a clear transition from ℓ_g^{dyn} to ℓ_g, which had *almost*, but

not completely, taken place by the time the equilibrium profile was measured. In fact, by fitting the time dependence of ℓ_g^*, we get an equilibrium value which is still about 17% lower than the experimental value $\ell_g = 188\ \mu$m reported in [3]. The fitted value would correspond to a particle radius $R \simeq 85$ nm, which is just 5% lower than the value $R = 90$ nm reported in [3]. A particle radius $R \simeq 85$ nm gives also a better agreement with numerical simulations of the profile time dependence. It is then presumable that the alleged 'anomaly' was due to a slight overestimate of R. The rather large discrepancy in the profile of the crystal branch, which for the samples used in [5] was found to equilibrate only for $t \gtrsim 8t_S$, further confirms that equilibrium was not yet fully reached. However, the second series of results presented in [3], referring to a number of samples prepared in widely different Φ_0 and ionic strength conditions, seemed to imply that the apparent value of ℓ_g could be even larger. Although the original data for this experiment are partly missing, it is very likely that in this case the profiles, which were followed for a much shorter settling time, were even further from equilibrium, so that the measured gravitational lengths were closer to ℓ_g^{dyn} than to ℓ_g (this would also qualitatively explain the apparent correlation with the sediment height reported in [3], since the kinetics is slower for thicker sediments). Although we do not claim to have fully solved the riddles raised by [3], we believe that the ideas presented in this paper may give a concrete contribution for a full explanation.

3. Materials and methods

3.1. Colloidal system

The samples we used are aqueous dispersions of polymer colloids made of MFA, a copolymer of tetrafluoroethylene with perfluoromethylvinylether (PF-VME). While polytetrafluoroethylene (PFTE) is a highly crystalline polymer, forming by emulsion polymerization of polydisperse rod-like particles, the addition of PF-MVE, bestowing a larger flexibility to the chains, yields spherical, monodisperse particles. In comparison to other standard latex particles, MFA colloids present some unique features, making them particularly suitable for sedimentation studies [13]:

- Their average refractive index is very close to that of water (a peculiar property of perfluorinated compounds, not shared by any hydrocarbon polymers), which makes performing experiments in concentrated *aqueous* suspensions feasible (therefore allowing us, for instance, to study also electrostatic effects).
- They have a high material density ($\rho_p \simeq 2.1$–2.2), which sensibly reduces the timescale of sedimentation experiments and yields a better accuracy in particle volume fraction determination by density measurements.
- More importantly, they still retain a noticeable degree of crystallinity. Since the percentage of flexible vinylether in the polymer composition is rather small, an MFA particle can indeed be roughly pictured as a collection of crystallites, embedded into an amorphous matrix. As a consequence, particles are optically anisotropic, and therefore scatter depolarized light. As we shall see, the depolarized scattering intensity can be used as a very sensitive probe of the concentration profile.

The specific materials we used are aqueous suspensions of Hyflon^{TM} MFA, produced by Solvay-Solexis (Milano, Italy) [14]. The original MFA latex was first extensively dialyzed to wash away the excess of surfactants and other additives used in the emulsion polymerization. A small amount of the nonionic surfactant Triton X100, which adsorbs on MFA particle surfaces, forming a compact stabilizing monolayer [15], allowing us therefore to screen electrostatic interactions by the addition of salt (MFA particles bear a negative surface charge, due to both the fluorinated carboxyl end groups of the polymer chains and to strongly adsorbed perfluorinated anionic surfactants), was then added to the dialyzed latex. The stabilized latex was then concentrated by slow sedimentation to get sample batches with particle volume fractions exceeding 20–30%. Partial or full matching of the particle and solvent refractive indexes, required to perform depolarized scattering measurements (see section 3.2), was obtained by adding appropriate amounts of urea. From measurements of the scattered intensity as a function of the solvent index of refraction n_s (the 'index-matching curve', see [13]), the average index of refraction of an MFA particle is found to be $n_p = 1.352 \pm 0.002$.

As we stated, the very high material density of MFA (combined with its lack of swelling in almost all inorganic and organic solvents) yields a fundamental advantage for absolute calibration of the particle concentration. When colloidal particles are directly synthesized in solution by emulsion/microemulsion polymerization (or, for silica, are grown by the Ströber process), the determination of the exact particle volume fraction is notoriously a delicate point, in particular for small values of $\rho_p - \rho_s$, mainly due to the uncertainty in the value of the exact particle density, caused by partial swelling or, for silica, by the porosity of the particle internal structure. Most quantitative measurements therefore rely on fixing Φ by comparison to the phase behaviour of a 'reference' system, such as, for instance, hard spheres. This procedure is generally sensible and internally self-consistent but, for colloidal systems where the phase behaviour is not known, a reliable absolute calibration for Φ is required. With the density value for MFA, the problem is already very much reduced. Since the particle average refractive index n_p can be found with a high degree of precision from the index-matching curve, a further check of the volume fraction values obtained by density measurements was made by measuring the suspension refractive index n and evaluating Φ as $(n - n_s)/(n_p - n_s)$. Sedimentation experiments also require careful measurements of the particle size. The particle radius was then obtained using both dynamic light scattering (DLS) and scanning electron microscopy (SEM), and further checked by measuring the Stokes sedimentation velocity for very dilute suspensions. Combining these independent measurements, we obtained a particle radius $R = 77 \pm 3$ nm.

3.2. Depolarized static light scattering (DSLS)

As discussed previously, MFA particles embed a collection of crystallites characterized by an anisotropic optical

polarizability tensor. Even if the latter are randomly oriented within the amorphous matrix, their limited number N_c (of the order of a few tens [13]) leads to an effective optical anisotropy of the whole particle which is only reduced by a factor of $1/\sqrt{N_c}$. As a consequence, the light scattered by MFA colloids has a component orthogonal to the polarization of the incident field. We give here only a brief summary of the theory of light scattering from partially crystalline particles, pointing for a comprehensive review to [13].

Assuming an incident field polarized along $\mathbf{n}_i$, and calling α the particle optical polarizability tensor, the field scattered with polarization direction $\mathbf{n}_f$ is proportional to $\langle \mathbf{n}_i \cdot \alpha \cdot \mathbf{n}_f \rangle$, therefore showing, besides a temporal phase modulation due to the particle translational motion, an *amplitude* modulation due to Brownian rotation. For simplicity, we shall model MFA particles as uniaxial birefringent scatterers, characterized by principal refractive indices $n_\parallel$ and $n_\perp$, and therefore by an average refractive index $n_p = (n_\parallel + 2n_\perp)/3$ and an optical anisotropy $\Delta n = n_\parallel - n_\perp$. Provided that the single crystallites within a particle are small compared to the wavelength, and assuming an incident polarization perpendicular to the scattering plane ('vertical' polarization), the horizontal (I_{VH}) and vertical (I_{VV}) polarization components of the intensity scattered by N interacting particles at wavevector q are (apart from unimportant multiplicative constants) [13]

$$\begin{aligned} I_{VH} &= N(\Delta n)^2 \\ I_{VV}(q) &= N\left[(n_p - n_s)^2 P(q) S(q)\right] + c I_{VH} \end{aligned} \tag{12}$$

where $P(q)$ is the particle form factor, $S(q)$ is the suspension structure factor and c is ideally equal to 4/3 for optically monodisperse particles, but is in practice usually larger due to fluctuations in the degree of crystallinity among the colloids (for MFA particles $c \simeq 2$) [13]. The main feature of equation (12) is that, at variance with I_{VV}, the depolarized intensity I_{VH} depends neither on the optical contrast $n_p - n_s$ nor on interparticle interactions, being actually q-independent. It is therefore a fully incoherent contribution (an optical analogue of incoherent neutron scattering), which is just proportional to the number of particles N in the scattering volume and can be then profitably exploited as a probe of the local particle concentration.

Our experimental apparatus basically consists of a custom-made light scattering set-up, operating at a fixed scattering angle $\vartheta = 90°$. Selection of the incident and detected polarization of the scattered intensity is made by means of two Glan–Thomson polarizers with an extinction ratio better than 1×10^{-6}. The cell is mounted on a DC-motorized micrometric translator, allowing cell positioning with a resolution of 0.1 μm and an absolute accuracy of about 3 μm. An He–Ne laser beam is mildly focused in the cell to a spot size $w = 46$ μm, corresponding to a depth of focus (Rayleigh range) of about 10 mm, fixing the maximum useful optical path in the cell. The whole set-up is enclosed in a removable hood allowing us to control temperature to better than 0.5 °C. Absolute volume fractions $\Phi(z)$ are obtained from $I_{VH}(z)$ by comparison with the depolarized intensity scattered by a calibration suspension. Since depolarized scattering from water is almost negligible, particle volume fractions as low as 10^{-5} can be easily detected. Since for MFA particles $\Delta n \sim 10^{-3}$, the coherent contribution to I_{VV} (the first term on the right-hand side of equation (12)) will, however, in general greatly exceed I_{VH}, unless $n_s \simeq n_p$. Working in quasi-index-matching conditions is then mandatory to avoid leakage of the polarized component through the analyser, or spurious contributions due to depolarized multiple scattering.

3.3. Beam deflection (BD)

DSLS is then a very sensitive and useful technique, but it necessarily relies on using optically anisotropic particles close to index-matching conditions. Unfortunately, most model colloidal systems (such as PMMA, silica or polystyrene particles) are amorphous, or hard to be suspended in an appropriate solvent, so that DSLS is presently suitable to be applied only to a very limited class of colloids (for aqueous suspensions, essentially only to lattices of PTFE copolymers). Here we discuss a laser beam deflection method (BD), which has been recently and successfully used to probe thermophoresis (colloidal motion induced by thermal gradients) in colloidal suspensions and complex fluids [16, 17], but can also be profitably exploited to obtain sedimentation profiles, with an accuracy comparable to DLS, for a much wider class of colloidal systems. BD is a simple and reliable experimental method which exploits the deflection of a laser beam propagating through a medium where a concentration, and therefore refractive index, gradient is induced by an external field[4]. From the equation for the propagation of rays in inhomogeneous media

$$\frac{\mathrm{d}}{\mathrm{d}s}\left(n(\mathbf{r})\frac{\mathrm{d}\mathbf{r}}{\mathrm{d}s}\right) = \vec{\nabla} n(\mathbf{r}), \tag{13}$$

where $\mathbf{r}$ identifies the ray trajectory parametrized by the curvilinear abscissa s and $n(\mathbf{r})$ is the refractive index, and assuming that the beam propagates along x in the presence of a weak gradient along z (so that $\mathrm{d}s \approx \mathrm{d}x$), the wavevector $\mathbf{k} = \mathrm{d}\mathbf{r}/\mathrm{d}s$ satisfies $\mathrm{d}\mathbf{k}/\mathrm{d}x \simeq \vec{\nabla} n/n$. Therefore the beam suffers an angular deflection with respect to the original propagation given by

$$\frac{\partial \theta}{\partial x} \simeq \frac{1}{n}\frac{\partial n}{\partial z}, \tag{14}$$

which is the basic equation relating the deflection of the beam to the imposed refractive index gradient.

A schematic description of our apparatus is the following. An He–Ne laser beam is mildly focused through the cell, which can be vertically translated, as in the DSLS apparatus, by a motorized actuator. The transmitted beam position is monitored by a position-sensitive detector with a resolution of 5 μm, placed at a distance $L \simeq 50$ cm from the cell. The beam position deflection Δz on the sensor is approximately given by

$$\Delta z \simeq \frac{\mathrm{d}n}{\mathrm{d}z} L l = L l \Delta n \frac{\mathrm{d}\Phi}{\mathrm{d}z}, \tag{15}$$

[4] A well-known and closely related phenomenon is the bending of light rays propagating through air that is optically inhomogeneous because of a thermal gradient, which is the origin of mirages.

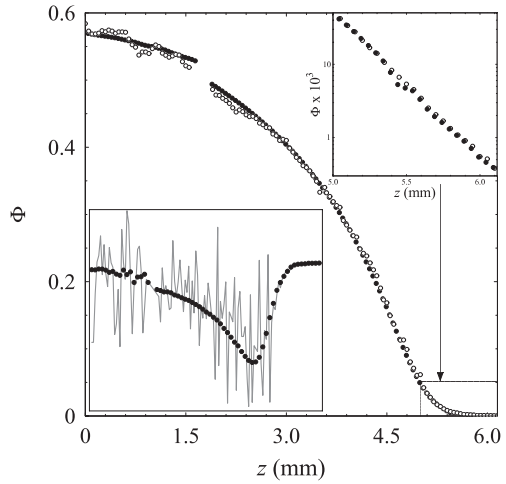

Figure 4. Main body: equilibrium sedimentation profiles for an HS system, obtained using either DSLS (○) or by numerical integration of the BD results (●). For BD data, the absolute position of the crystal branch has been fixed by superposition on the DSLS results (see text). The lower-left inset shows that the original BD data (●) are much less noisy than the numerical derivative of the DSLS profile (grey line). The barometric regions of both profiles are shown in the upper-right inset on a log plot.

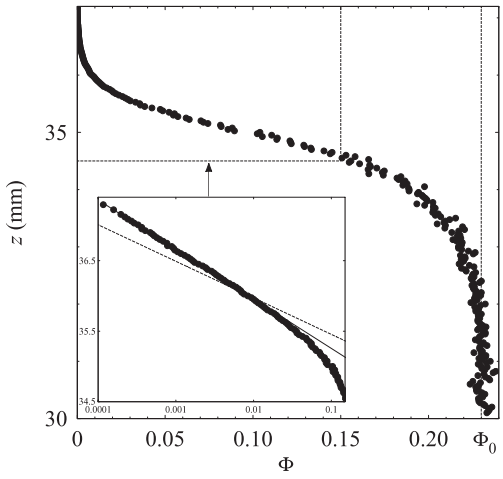

Figure 5. Stationary settling profile for an MFA suspension at $\Phi_0 = 0.23$ in the presence of 100 mM NaCl, obtained by DSLS (●). The corresponding log plot in the inset shows that ℓ_g^{dyn}, given by the slope of the full line, is sensibly larger than ℓ_g (dashed line).

where $\Delta n = n_p - n_s$ and $l = 1$ cm is the optical path in the cell, yielding a minimum appreciable refraction index gradient $dn/dz \simeq 10^{-9}\mu m^{-1}$. For MFA particles with $\ell_g \simeq 200\ \mu m$ in water ($\Delta n \simeq 0.02$), the minimum measurable value of Φ in the barometric region, where $\partial\Phi/\partial z = \Phi/\ell_g$, is of the order of 10^{-5}.

Since equation (15) is linearly proportional to the *derivative* of the concentration profile, to obtain the equation of state BD data must be integrated twice. While this is not a problem for smooth profiles (on the contrary: the additional integration helps smoothing noisy data), it is a clear disadvantage when dealing with discontinuous profiles. Indeed, the exact amount of the concentration jump at the meniscus separating two phases, where dn/dz is undefined, cannot be extracted, so that BD measurements alone cannot yield quantitative phase equilibria. Yet, according to the discussion made in section 2.2, a direct measurement of $d\Phi/dz$ can be a major advantage when inverting settling profiles to extract $K(\Phi)$. When dealing with turbid samples, BD also has the crucial advantage that multiple scattering is not a severe problem. Indeed, provided that a detectable amount of transmitted beam reaches the sensor, and that the latter is placed at sufficiently long distance from the cell to limit the collection of light scattered at small angles, the method works even for quite turbid samples.

4. Experimental results

4.1. Equilibrium profiles

Sedimentation measurements by DSLS have extensively and successfully been used to gain detailed information on the phase behaviour of colloids interacting via short-ranged depletion forces induced by nonionic surfactant micelles [5] but, as discussed in section 3, they are unavoidably limited to suspensions of optically anisotropic particles. For what concerns equilibrium profiles, here we shall only dwell upon the openings provided by an alternative method such as beam deflection. Equilibrium profiles obtained for a stabilized MFA suspension at $\Phi_0 = 0.23$, in the presence of about 100 mM NaCl, are compared in figure 4. The sample was prepared in slightly out-of-matching conditions ($n_p - n_s \simeq 0.003$) to allow simultaneous measurement by DSLS and BD. The main body of the figure shows that the fluid branches of the two profiles essentially coincide, demonstrating the effectiveness of the BD method, which yields an even less noisy profile due to the smoothing intrinsically associated with integrating $d\Pi/dz$. Also, as the upper-right inset shows, BD allows us to measure the very dilute barometric part of the profile with an accuracy comparable to DSLS. As we discussed in section 3.3, however, BD is not capable to quantitatively account for discontinuities at phase boundaries. Indeed, the absolute position of the solid branch of the BD profile has been fixed by imposing a concentration jump equal to that one measured with DSLS. The agreement of the two profiles in this region seems, however, slightly poorer. The original BD data are compared with the very noisy numerical derivative of the DSLS profile in the lower-left inset of figure 4, which clearly shows that DSLS is definitely not the most efficient method to extract dynamic information from a settling profile according to the method discussed in section 2.2.

4.2. Settling profiles

As a first illustration of the idea presented in section 2.2 we show in figure 5 a DSLS settling profile for the HS suspension described in the former paragraph, measured after the time-invariant shape is reached. The inset shows that the logarithmic slope of the dilute top part of the profile is about 35% larger than its equilibrium value. In figure 6 we show how the concentration dependence of $K(\Phi)$ can be

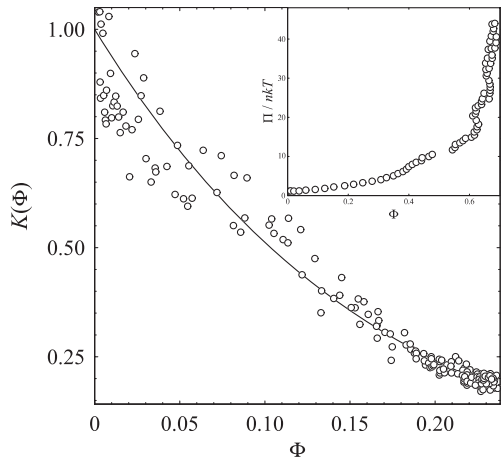

Figure 6. Hydrodynamic factor $K(\Phi)$ obtained from settling profile of figure 5 (○). The equation of state, obtained by integrating the equilibrium profile in figure 4 and used to invert the profile, is shown in the inset.

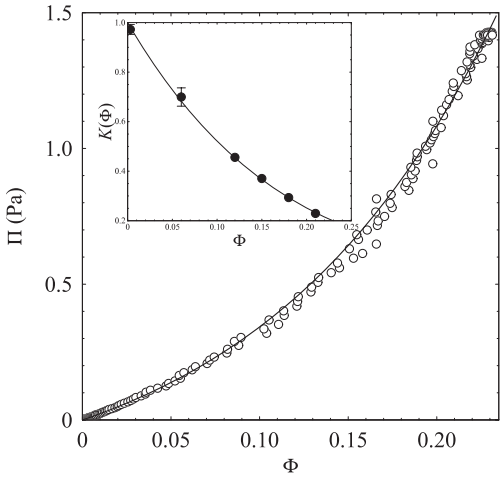

Figure 7. Comparison of the CS equation of state (full line) to the results obtained from settling profile of figure 5 (○) using the data for $K(\Phi)$ shown in the inset (obtained by simply video-tracking the time displacement of the meniscus). The full line is the fit to $K(\Phi)$ discussed in the text and used to invert the profile.

directly extracted from the settling profile in figure 5 using the experimental equation of state obtained from measurements of the equilibrium sedimentation profile. The full line is a fit of the hydrodynamic factor of the form, yielding, however, $b = 6.35 \pm 0.10$, an exponent which is slightly lower than the semi-empirical value $b = 6.55$ obtained by extrapolating to high concentration Batchelor's result [18] for the virial coefficient of v_s.

A single static measurements of the settling profile for a concentrated suspension is therefore a valid substitute for extensive measurements of the sedimentation velocity as a function of Φ, in particular since sedimentation velocity measurements require careful temperature control to avoid fluctuations of the solvent viscosity. Conversely, if the latter have been performed, and therefore $K(\Phi)$ is known, settling profiles directly yield the system equation of state up to Φ_0. To show this, we have measured the sedimentation velocity of MFA suspensions as a function of concentration by macroscopically tracking for a long time with a CCD camera the position of the meniscus (corresponding to the thin fan region) separating the settling suspension from the supernatant. The results, shown in the inset of figure 7, are well fitted by $K(\Phi) = (1 - \Phi)^b$, with an exponent $b = 6.22 \pm 0.08$, which is quite close to the value obtained in figure 6. This expression for $K(\Phi)$ has then been used to get from the profile in figure 4 the equation of state up to $\Phi = 0.23$, which is shown in the main body of figure 7. Consistently, the experimental $\Pi(\Phi)$ agrees pretty well with the CS equation of state, given by the full line. If this method does not obviously yield new information for hard spheres, it could be rather used to obtain results for colloidal suspensions with a unknown equation of state, without waiting for long equilibration times.

4.3. Dynamic sedimentation length

All we have discussed so far refer to HS, which we have selected as a particularly well-known model. To test the predictions for ℓ_g^{dyn} made in section 2.2, we prefer presenting

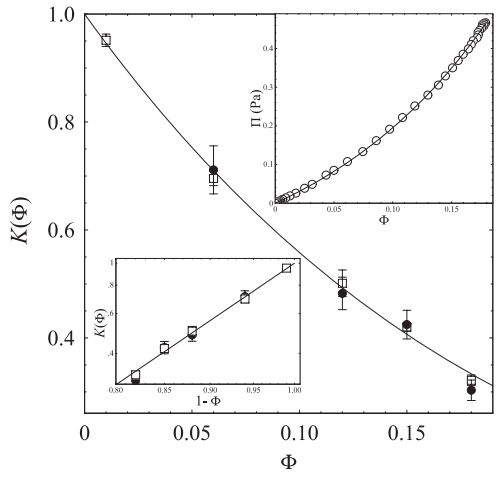

Figure 8. Concentration dependence of the hydrodynamic factor $K(\Phi)$ for MFA suspensions in the presence of a volume fraction $\Phi_s = 0.05$ of added Triton X100, obtained either by standard measurements of the settling velocity (□) or from the measured values of l_g^{dyn} (●). The full line is a fit with $K(\Phi) = (1 - \Phi)^{5.5}$ (which can be better appreciated in the double log plot shown in the lower-left inset). The upper-right inset shows the equation of state derived according to the text using the former expression for $K(\Phi)$.

some preliminary data obtained for MFA suspensions where depletion forces are induced by the presence of micellar aggregates of the nonionic surfactant Triton X100. Due to the very short-ranged nature of the attractive interaction potential, the equation of state and phase behaviour of this system, which have been extensively studied in [5], closely conform to the predictions made for adhesive hard spheres. We have prepared five MFA suspensions with particle volume fractions varying in the range $0.01 < \Phi < 0.18$, at fixed surfactant volume fraction $\Phi_s = 0.05$. With the exception of the most dilute sample ($\Phi = 0.01$) all profiles reached a time-invariant shape, allowing us to obtain ℓ_g^{dyn} from DSLS measurements of the profile. Figure 8 shows that hydrodynamic factors calculated

either from direct measurements of the sedimentation velocity or from the values of l_g^{dyn} via equation (11) agree quite well. Although the number of data points is quite limited, $K(\Phi)$ seems to behave (see inset) as $(1-\Phi)^b$, similarly to HS, but with an exponent $b \simeq 5.5$. The latter can be roughly accounted for by the theoretical predictions for the sedimentation velocity of sticky HS [19], yielding, for sufficiently low concentration, $v(\Phi) = v_s(1 - 6.546\Phi + 0.875/\tau)$, where τ is the stickiness parameter measuring the strength of the attractive interaction in Baxter's AHS model [20]. The inset of figure 8 shows that the experimental $\Pi(\Phi)$ obtained from the settling profile of the most concentrated sample ($\Phi = 0.18$), using the former expression for $K(\Phi)$, is very well fitted by the equation of state for AHS [21] with a Baxter parameter $\tau = 1.0 \pm 0.2$. Using this value for τ, one would then expect $v(\Phi) = v_s[1 - (5.57 \pm 0.18)\Phi]$, in good agreement with the experimental results.

References

[1] Schuck P 2000 *Biophys. J.* **78** 1606
[2] Perrin J 1910 *J. Physique* **9** 5
[3] Piazza R, Bellini T and Degiorgio V 1993 *Phys. Rev. Lett.* **71** 4267
[4] Rutgers M A, Dunsmuir J H, Xue J-Z, Russel W B and Chaikin P M 1996 *Phys. Rev.* B **53** 5043
[5] Buzzaccaro S, Rusconi R and Piazza R 2007 *Phys. Rev. Lett.* **99** 098301
[6] Lu P J, Zaccarelli E, Ciulla F, Schofield A B, Sciortino F and Weitz D A 2008 *Nature* **453** 499
[7] Segre P N, Herbolzheimer E and Chaikin P M 1997 *Phys. Rev. Lett.* **79** 2574
[8] Mucha P J, Tee S Y, Weitz D A, Shraiman B I and Brenner M P 2004 *J. Fluid Mech.* **501** 71
[9] Russel W B, Saville D A and Schowalter W R 1992 *Colloidal Dispersions* (Cambridge: Cambridge University Press) chapter 12
[10] Esipov S E 1995 *Phys. Rev.* E **52** 3711
[11] Tee S-Y, Mucha P J, Brenner M P and Weitz D A 2008 *J. Fluid Mech.* **596** 467
[12] Carnahan N F and Starling K E 1969 *J. Chem. Phys.* **51** 635
[13] Degiorgio V, Piazza R, Bellini T and Visca M 1994 *Adv. Colloid Interface Sci.* **48** 61
[14] Solvay–Solexis, Technical Library http://www.solvaysolexis.com/services/tds
[15] Piazza R and Degiorgio V 1992 *Opt. Commun.* **92** 45
[16] Piazza R and Guarino A 2002 *Phys. Rev. Lett.* **88** 208302
[17] Braibanti M, Vigolo D and Piazza R 2008 *Phys. Rev. Lett.* **100** 108303
[18] Batchelor G K 1972 *J. Fluid Mech.* **52** 245
[19] Cichocki B and Felderhof B U 1990 *J. Chem. Phys.* **93** 4427
[20] Baxter R 1968 *J. Chem. Phys.* **49** 2770
[21] Barboy B and Tenne R 1979 *Chem. Phys.* **38** 369